Supporting Information

Non-solvating, side-chain polymer electrolytes as lithium single-ion conductors: synthesis and ion transport characterization

Jiacheng Liu,[1] *Phillip D. Pickett,*[2] *Bumjun Park,*[1] *Sunil P. Upadhyay,*[1] *Sara V. Orski,*[2] and *Jennifer L. Schaefer*[1]*

1. Department of Chemical and Biomolecular Engineering, University of Notre Dame, Notre Dame, IN, United States

2. Materials Science and Engineering Division, Material Measurement Laboratory, National Institute of Standards and Technology, Gaithersburg, MD, United States

Contents

List of abbreviations

ATR-FTIR – attenuated total reflectance - Fourier transform infrared

DCM – dichloromethane

DMSO – dimethyl sulfoxide

DMSO-d_6 – fully deuterated dimethyl sulfoxide

DSC – differential scanning calorimetry

GPC – gel permeation chromatography

LiPSTFSI - lithium poly(4-styrenesulfonyl(trifluoromethylsulfonyl)imide)

M_n – number averaged molecular mass

M_w – mass averaged molecular mass

NMR – nuclear magnetic resonance spectrum

Discussion of synthesis of poly-**6**, poly-**7**, oligo-**2**, and associated intermediates in accordance with **Scheme 1**.

Each monomer synthesis requires 5 steps (2 steps for compound **2**). The first step is the ether bond formation between 2,5-dichlorophenol and 1,10- dibromodecane to synthesize compound **1**. An excess amount of the dibromo- precursor was used to suppress the formation of the dimer side-product, which can be easily removed by extraction with methanol. The reaction was achieved with good yield (66 %). Synthesis of compound **3** took a longer time (24 h) due to the low solubility of **2** in water/ethanol. A DCM wash of the solid product was used to remove any unreacted precursors and possible dimer from this step to ensure no effect on the final polymerization. The following steps (iv and v) are all achieved in nearly quantitative yield for compound **6**. The lower yield in step (v) for compound **7** was because of its increased solubility in chloroform due to the tethered phenyl group. For the last step, the triethylammonium cation was exchanged to Li^+ to prevent dissociation to free triethylamine and subsequent chelation to the nickel catalyst center.

The polymer end group as result of the Negishi coupling reaction is -ZnCl, which is simultaneously hydrolyzed after acid quenching. As a result of excess of Zn^{2+} in the reaction mixture, most of the Li^+ counterion was replaced by Zn^{2+}. The zinc exchanged polymer can be precipitated in water due to the stronger interaction between Zn^{2+}. Drying at 180 °C under vacuum for 24 h is necessary to remove all of the solvent that coordinates with the Li^+. The polymers are hard solids with a dark red to brown color.

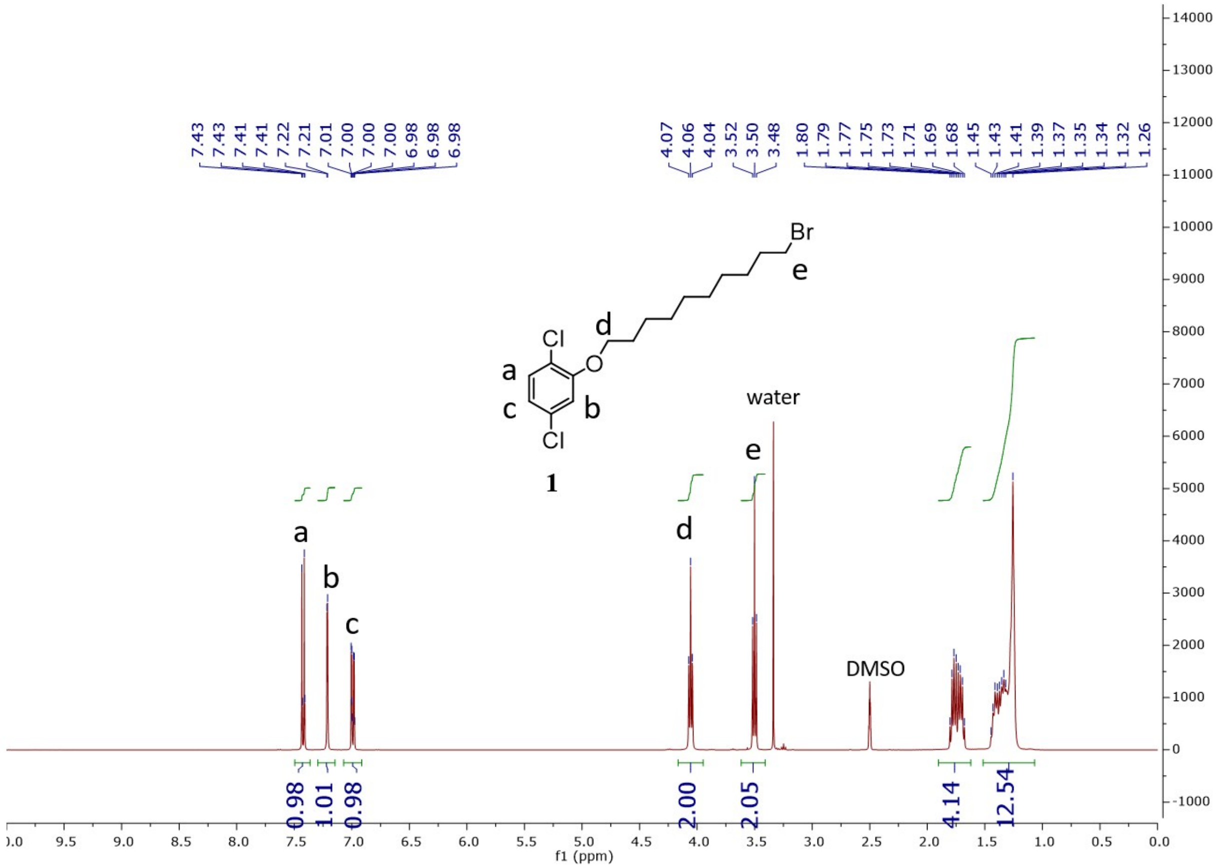

Figure S1. ^{1}H NMR of **1** in DMSO-d_6.

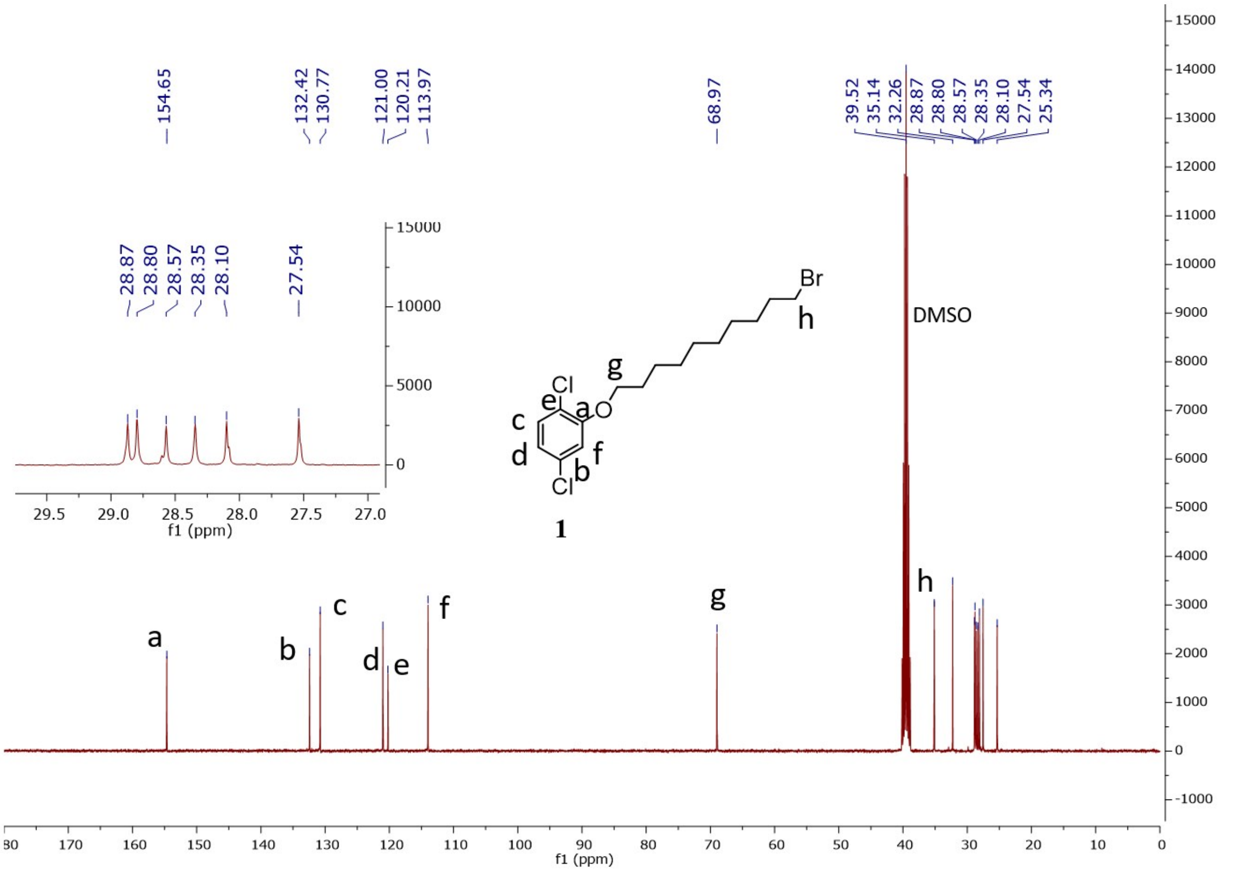

Figure S2. ^{13}C NMR of **1** in DMSO-d_6.

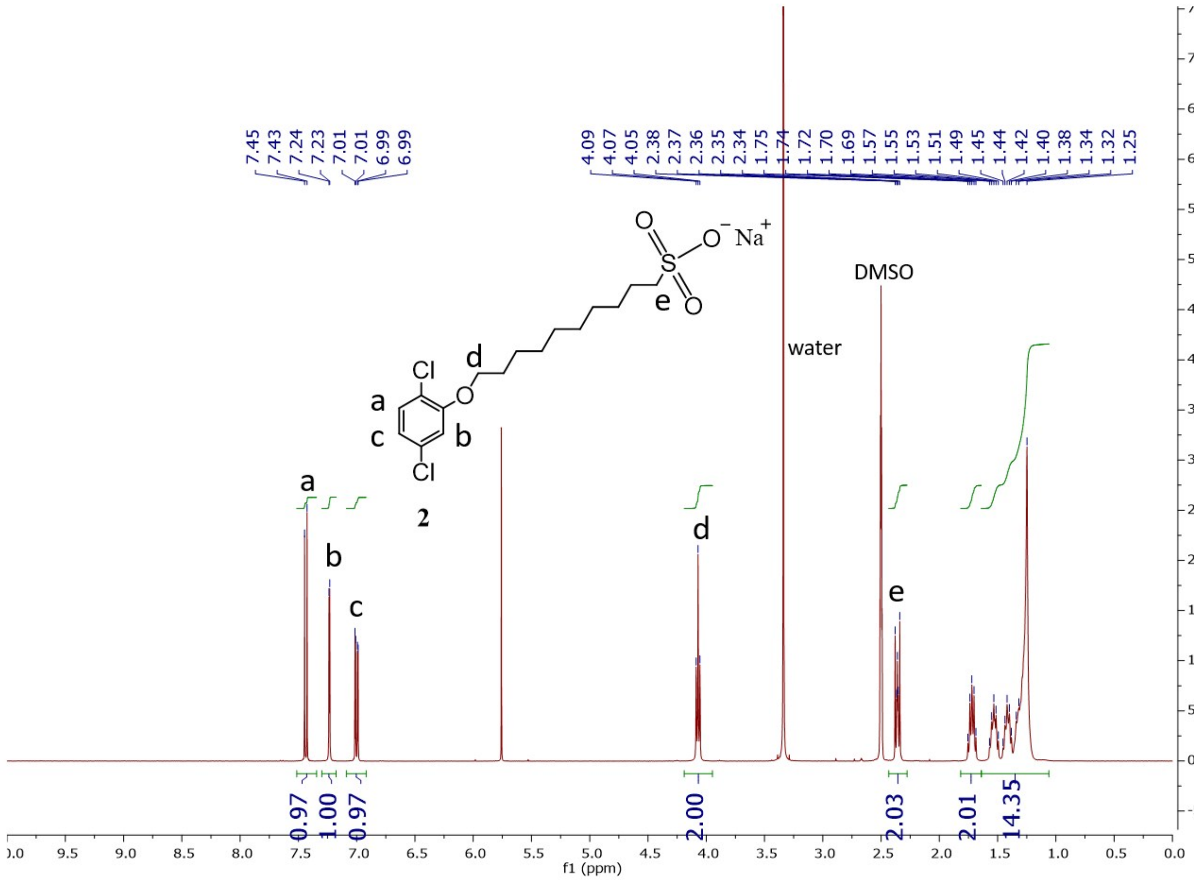

Figure S3. ^{1}H NMR of **2** in DMSO-d_6.

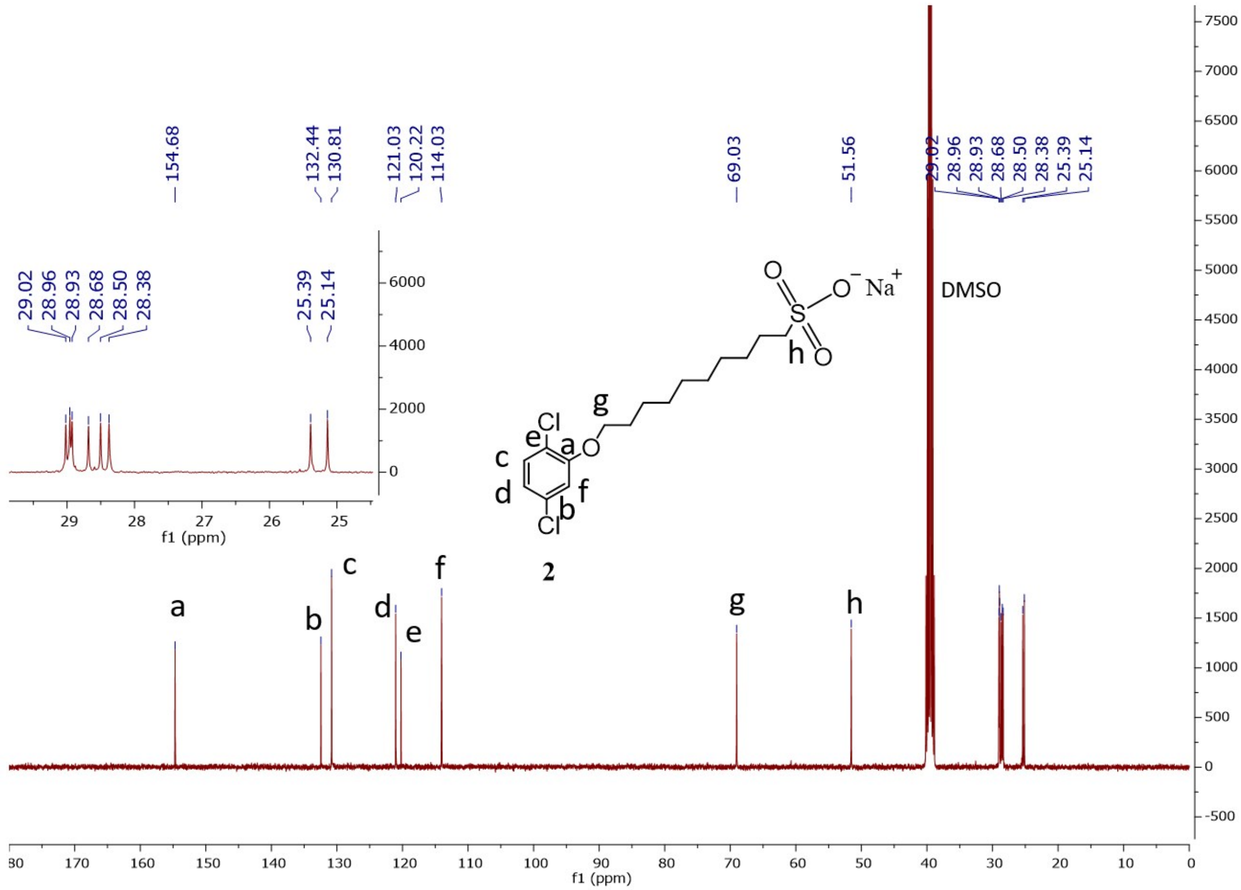

Figure S4. ^{13}C NMR of **2** in DMSO-d_6.

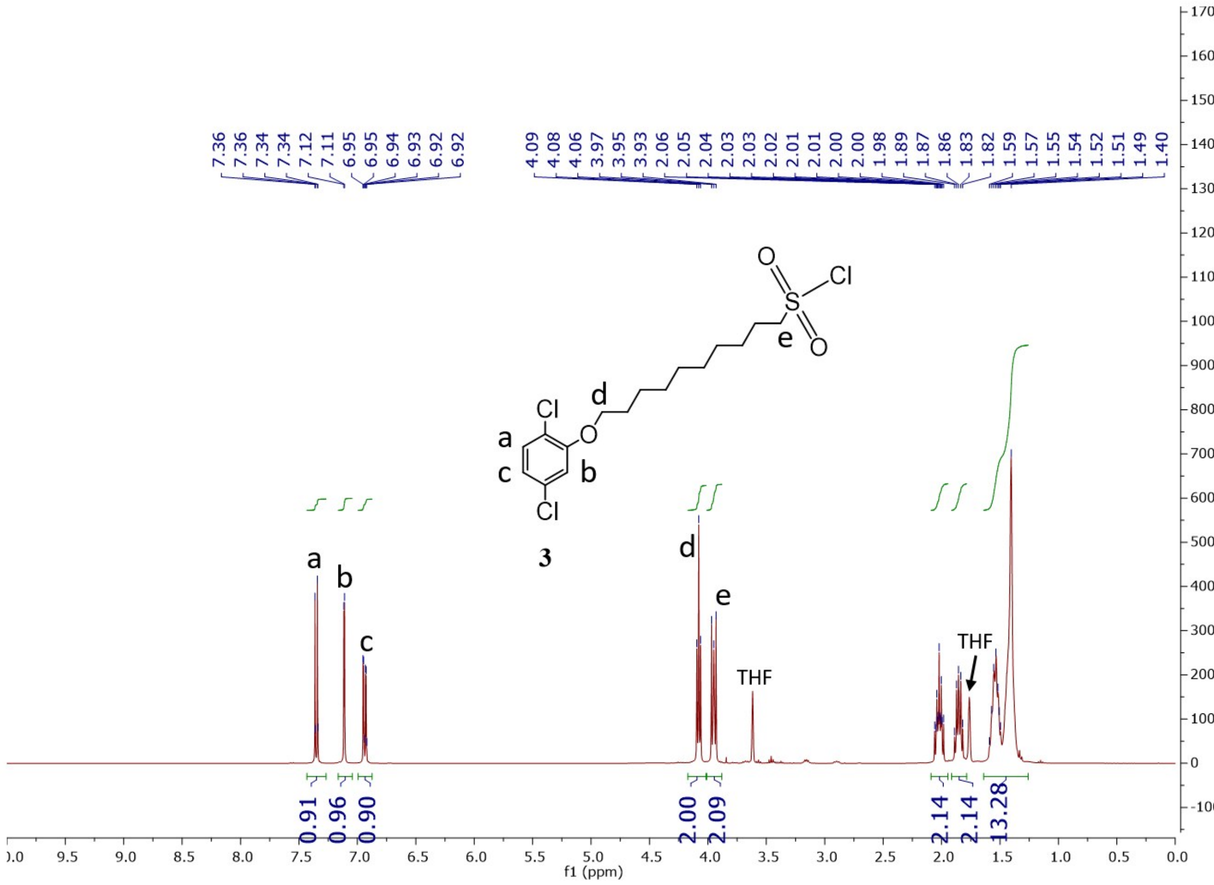

Figure S5. ^{1}H NMR of **3** in DMSO-d_6.

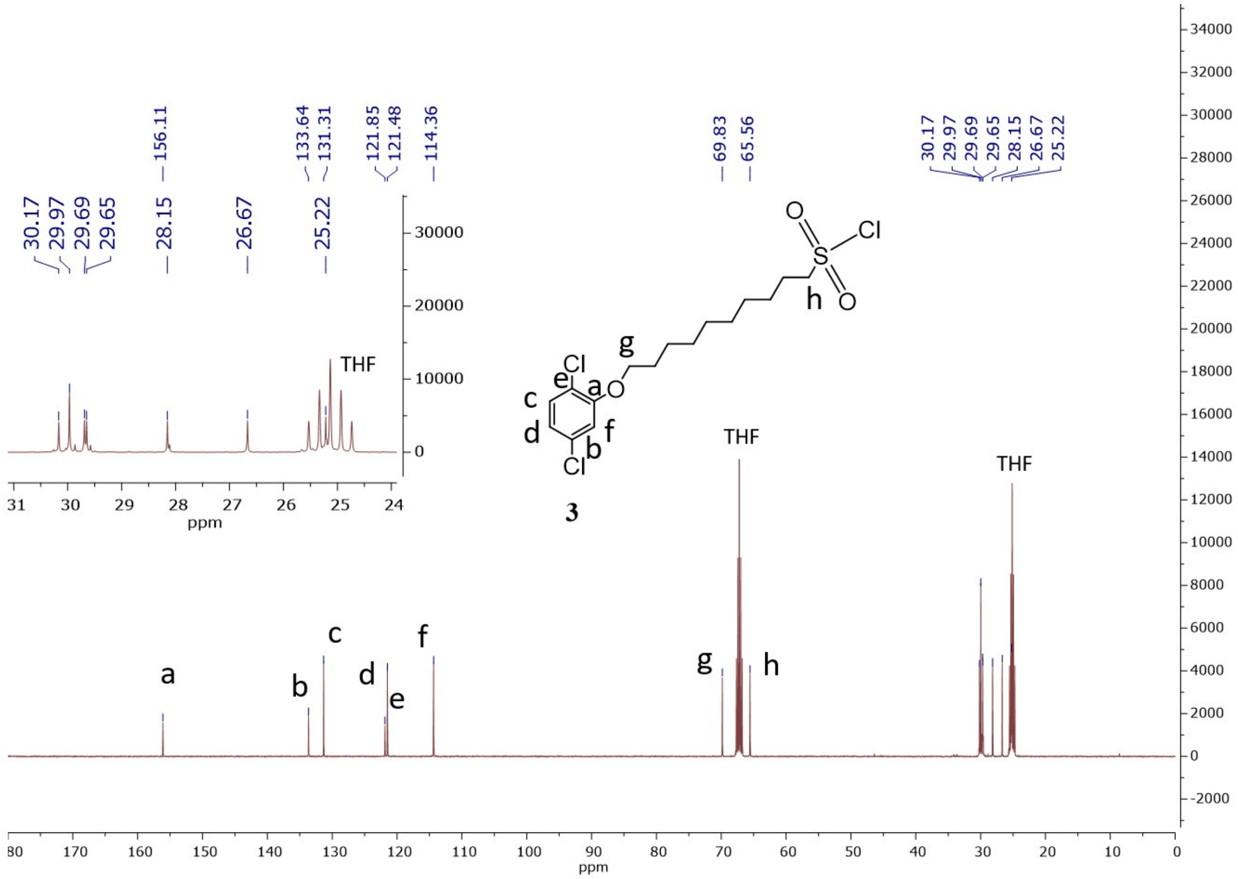

Figure S6. ^{13}C NMR of **3** in DMSO-d_6.

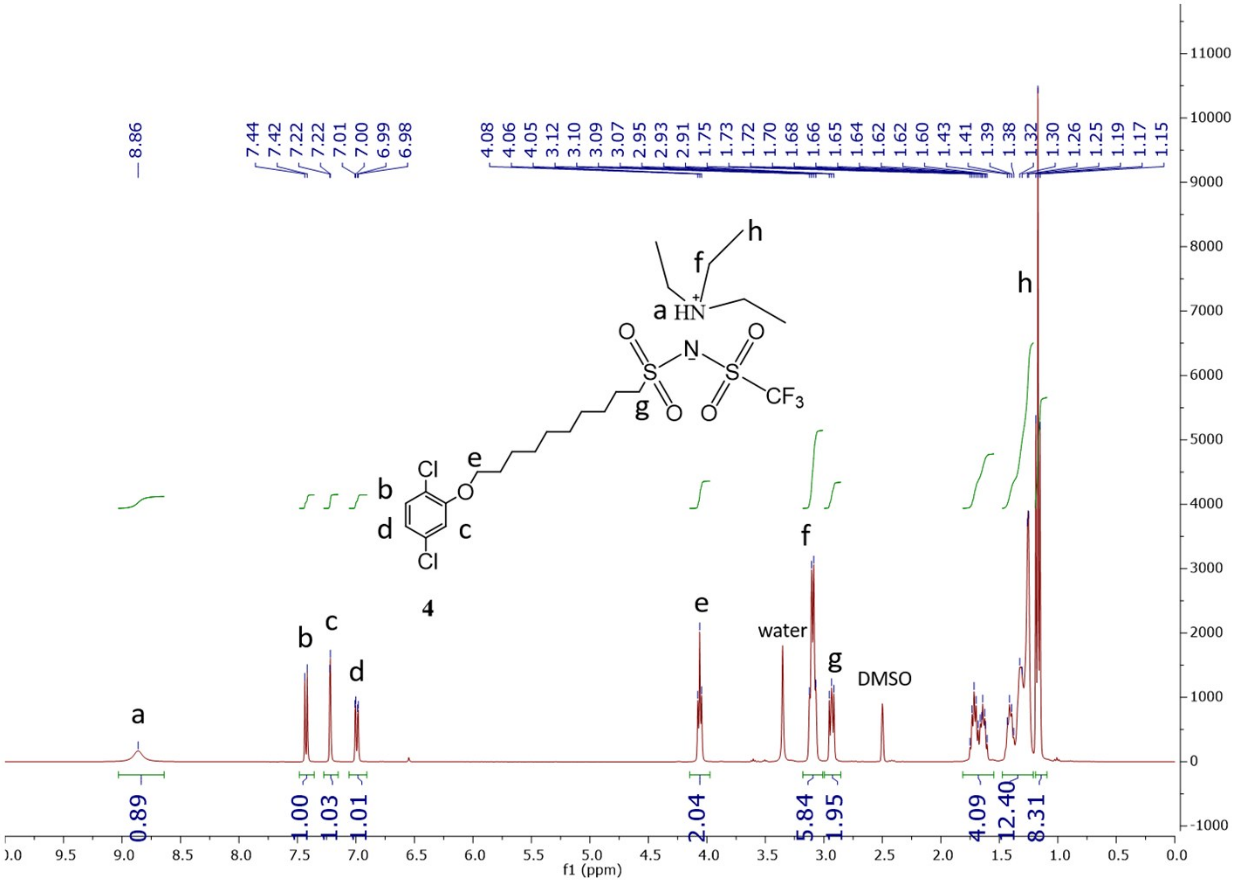

Figure S7. ^{1}H NMR of **4** in DMSO-d_6.

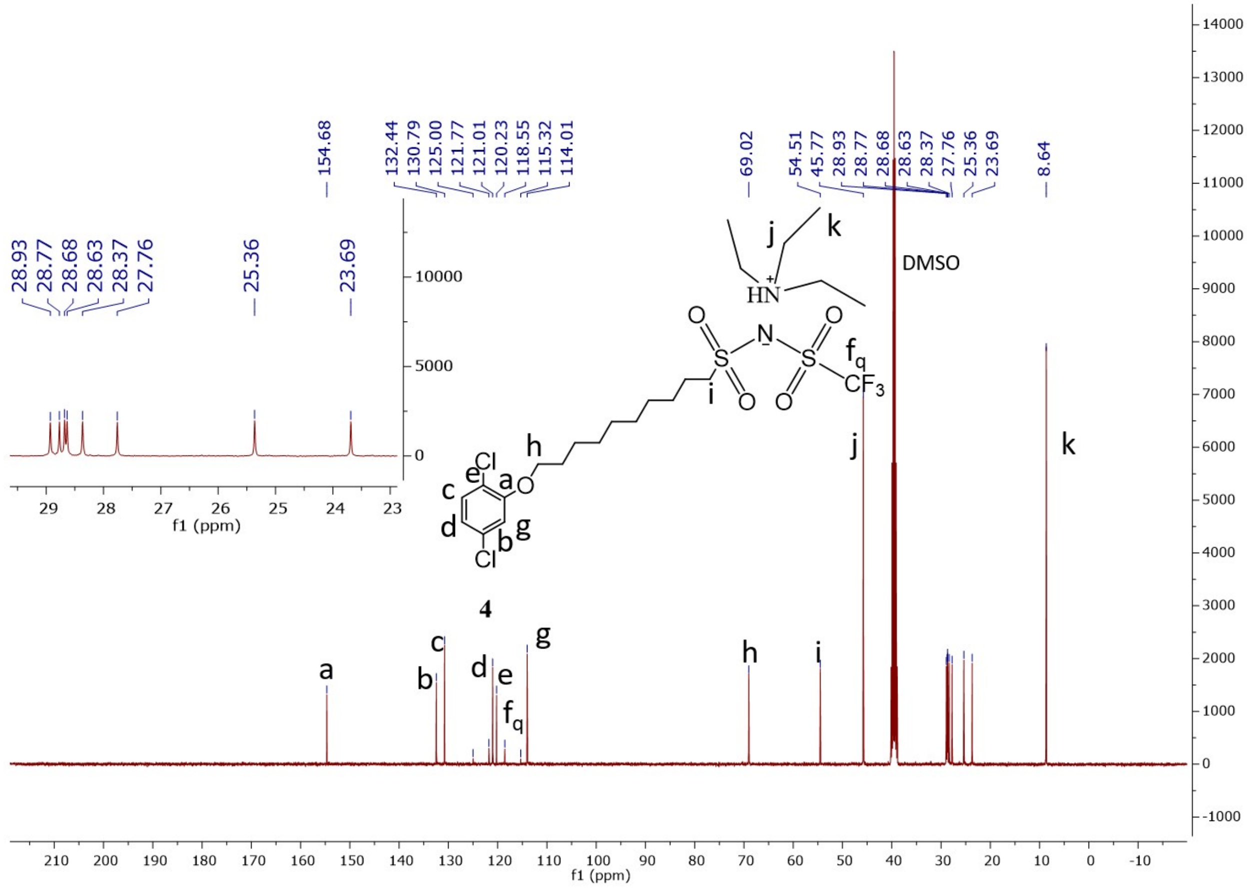

Figure S8. ^{13}C NMR of **4** in DMSO-d_6.

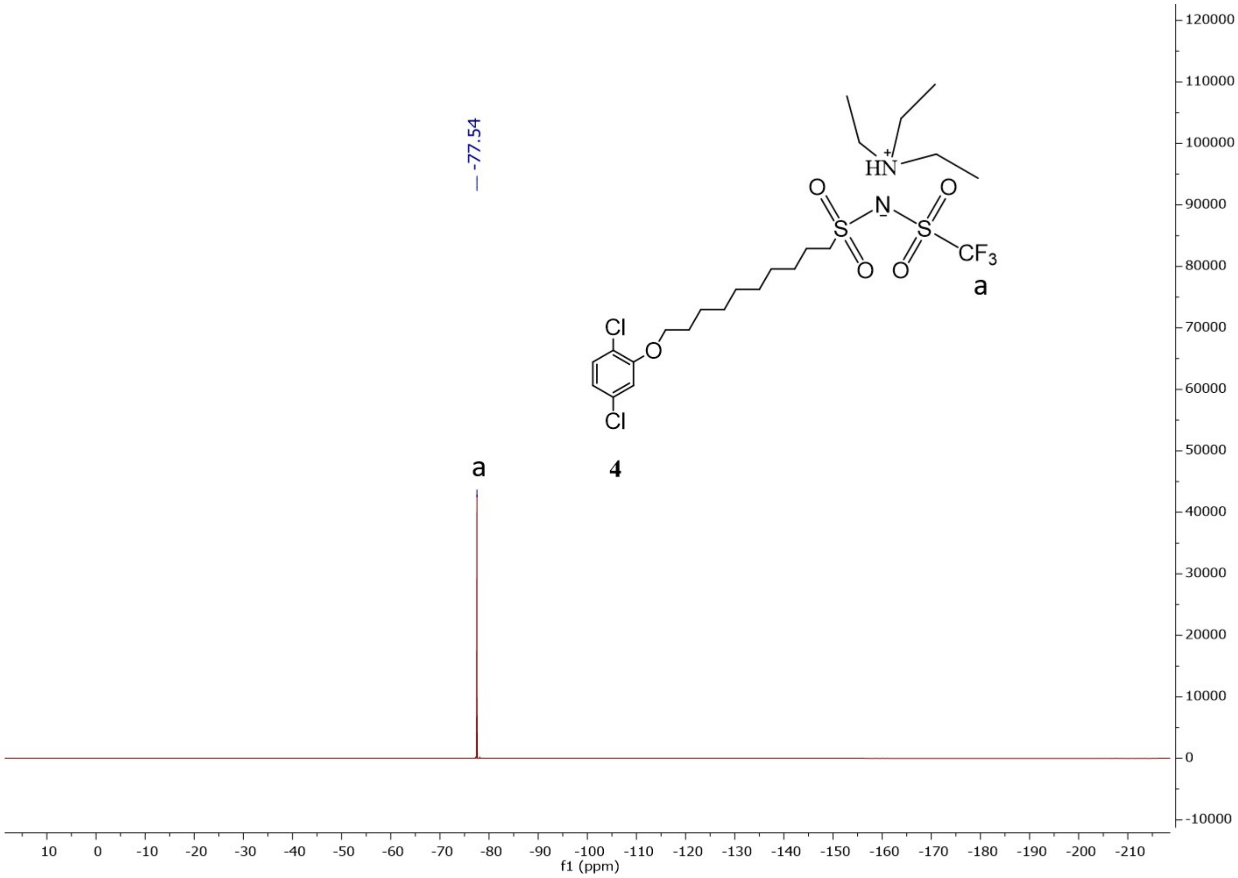

Figure S9. ^{19}F NMR of **4** in DMSO-d_6.

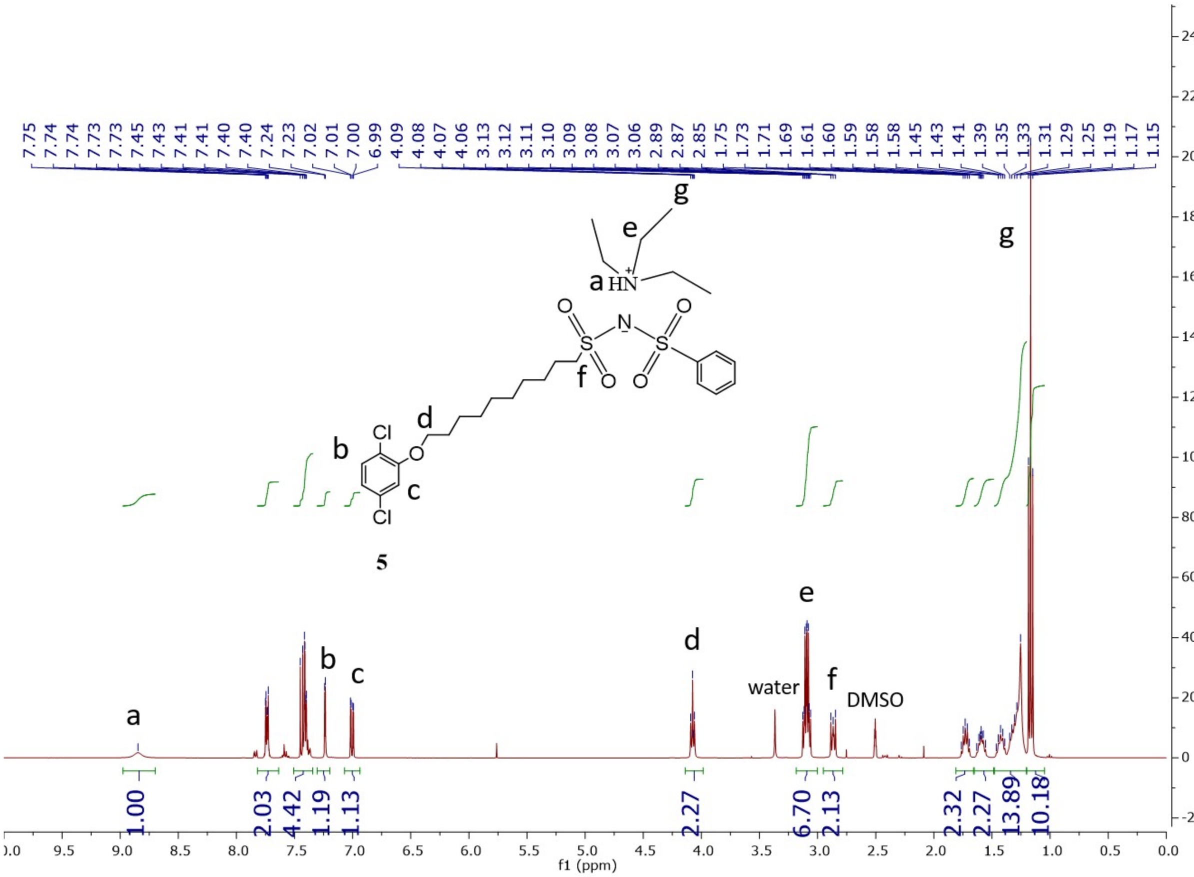

Figure S10. ^{1}H NMR of **5** in DMSO-d_6.

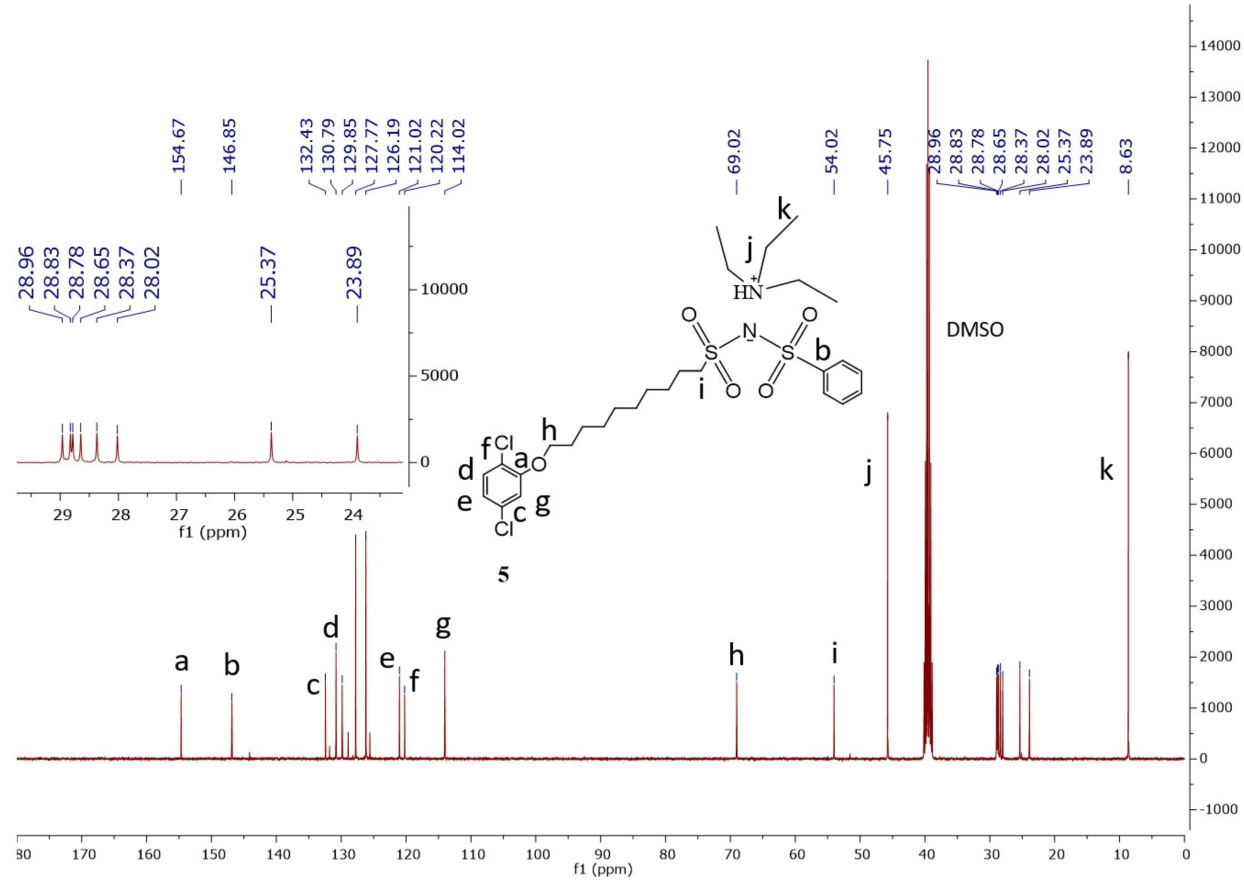

Figure S11. ^{13}C NMR of **5** in DMSO-d_6.

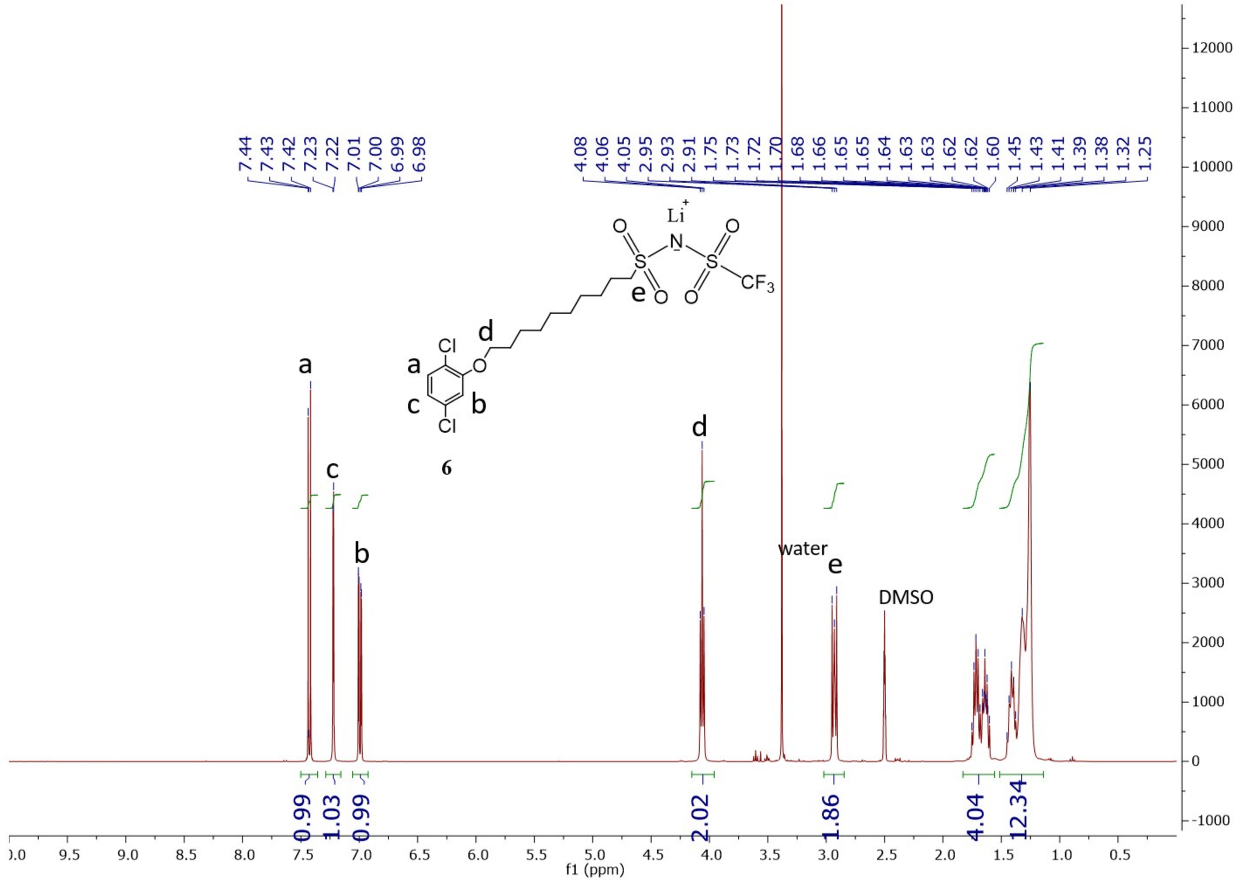

Figure S12. ^{1}H NMR of **6** in DMSO-d_6.

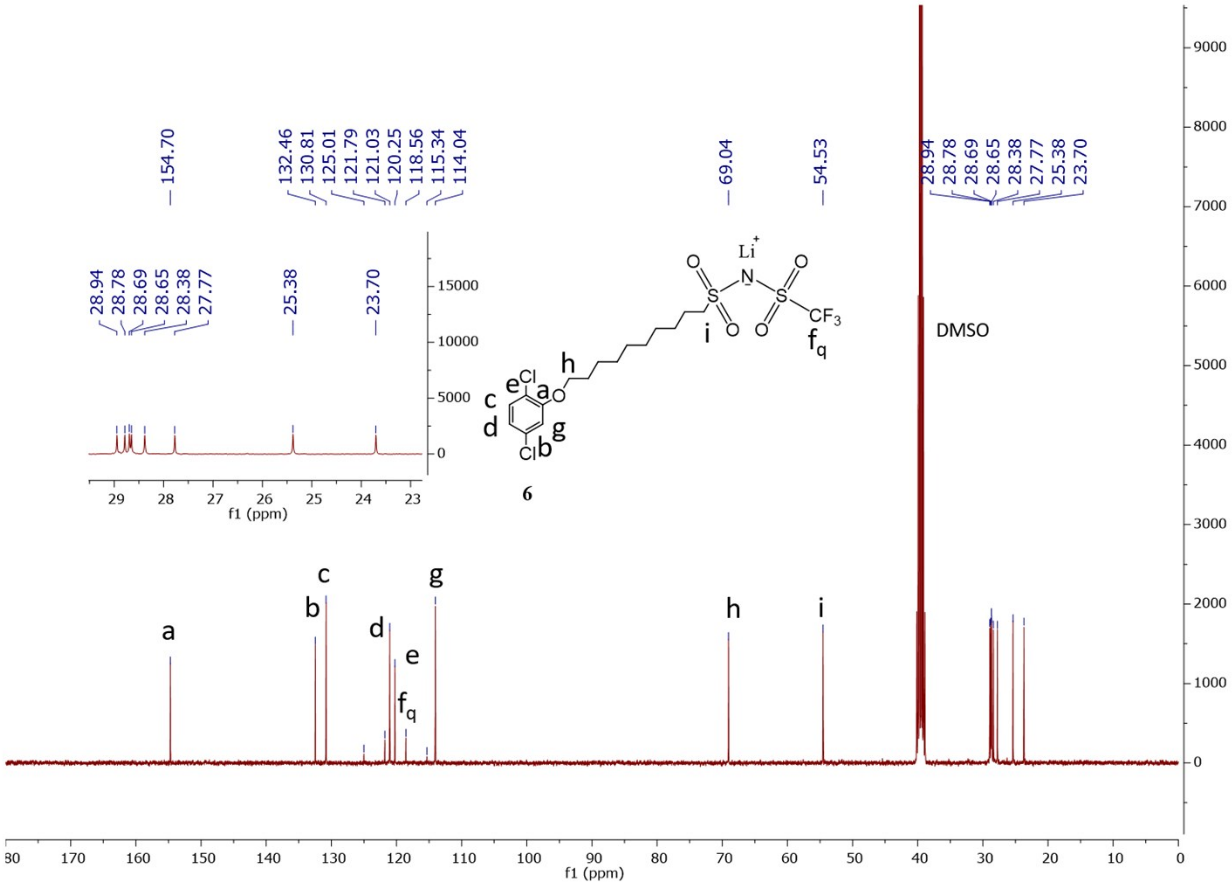

Figure S13. ^{13}C NMR of **6** in DMSO-d_6.

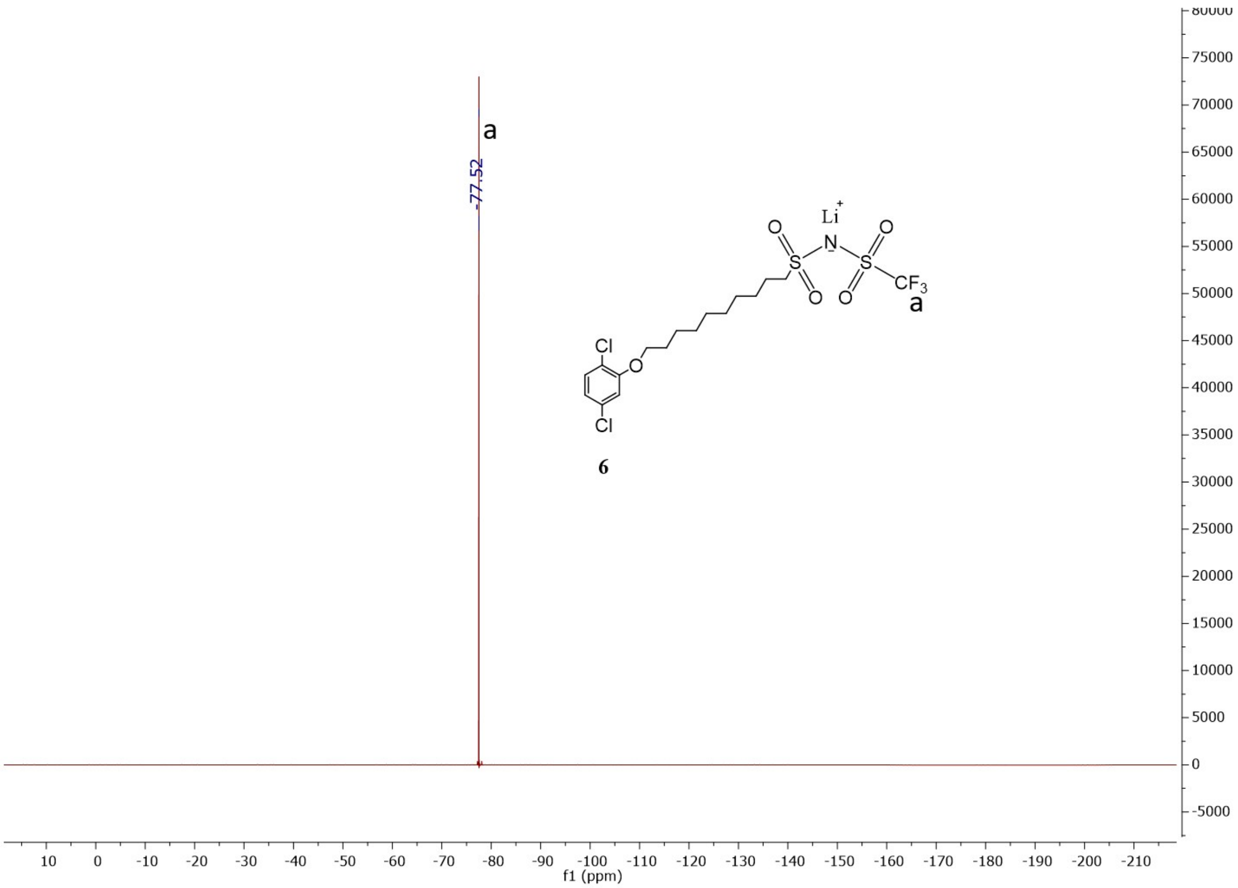

Figure S14. ^{19}F NMR of **6** in DMSO-d_6.

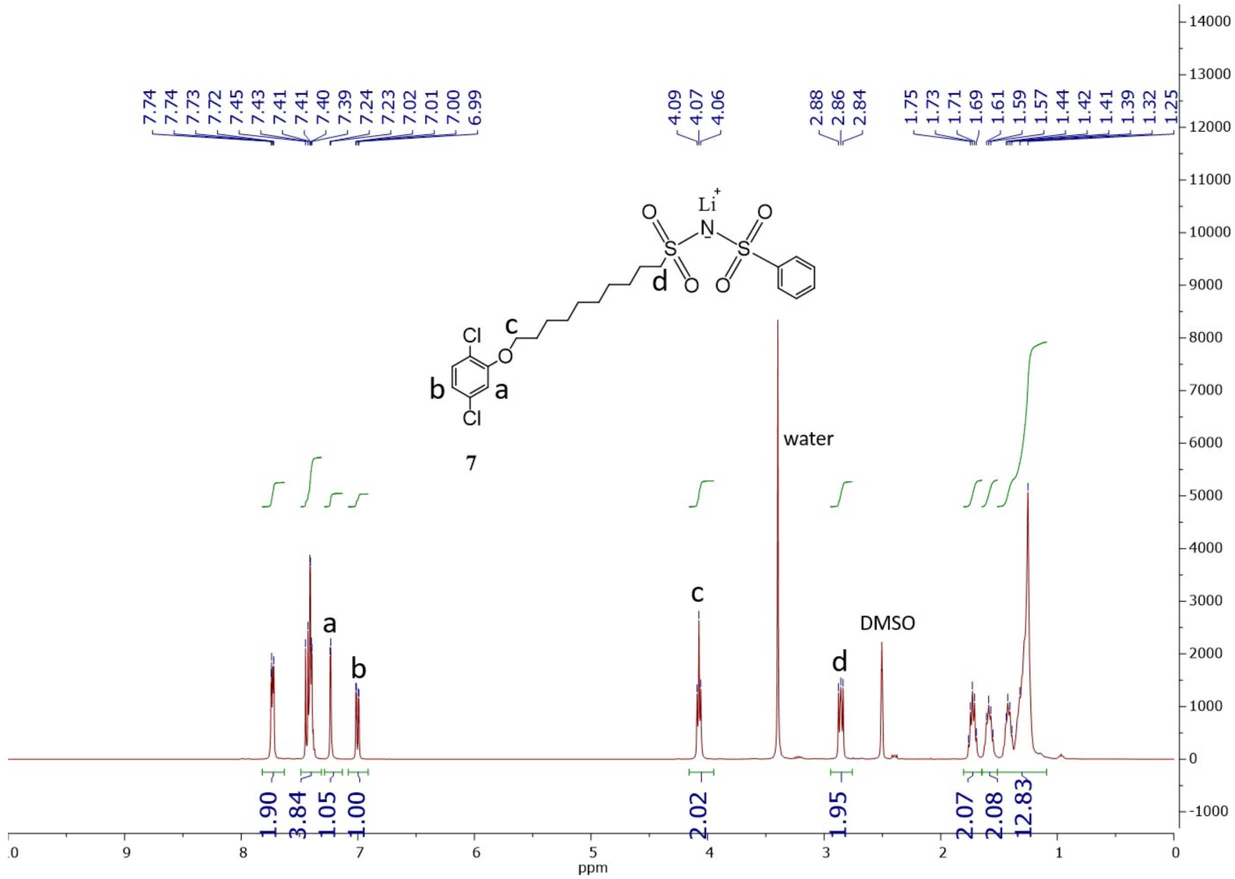

Figure S15. ^{1}H NMR of **7** in DMSO-d_6.

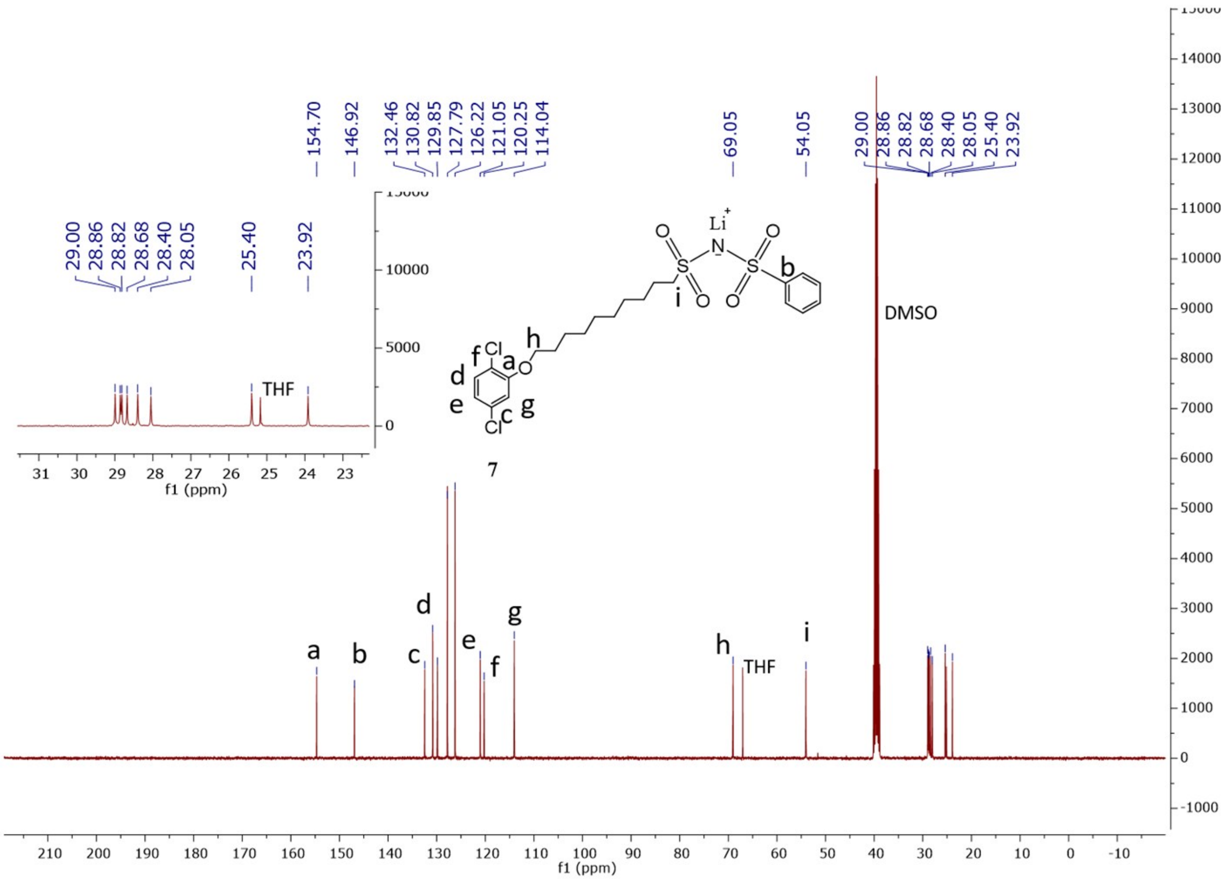

Figure S16. ^{13}C NMR of **7** in DMSO-d_6.

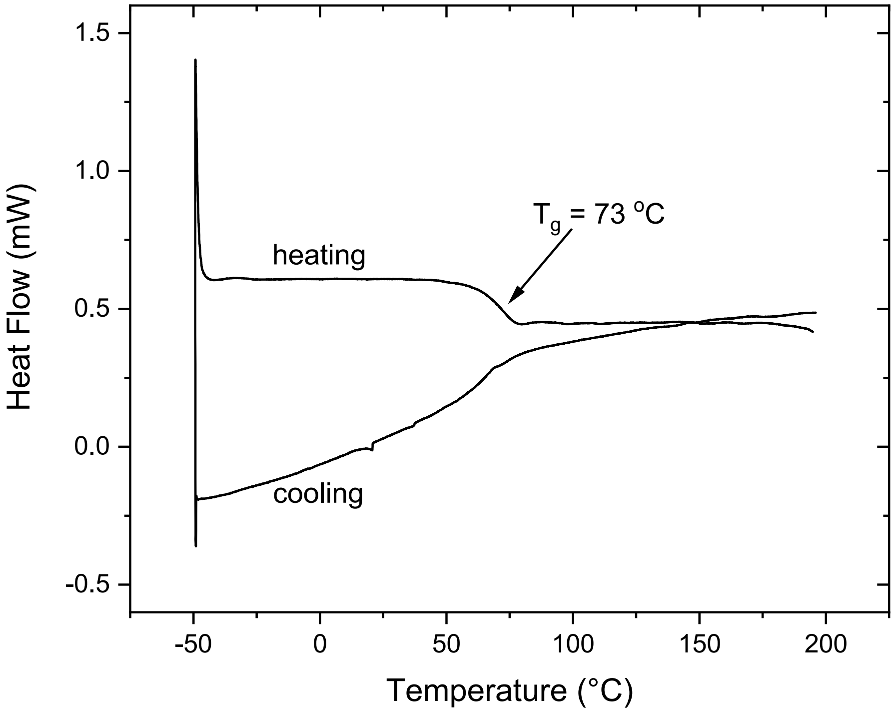

Figure S17. DSC thermogram of poly-6 at ramp rate of 10 °C/min. The glass transition temperature was determined on the heat run.

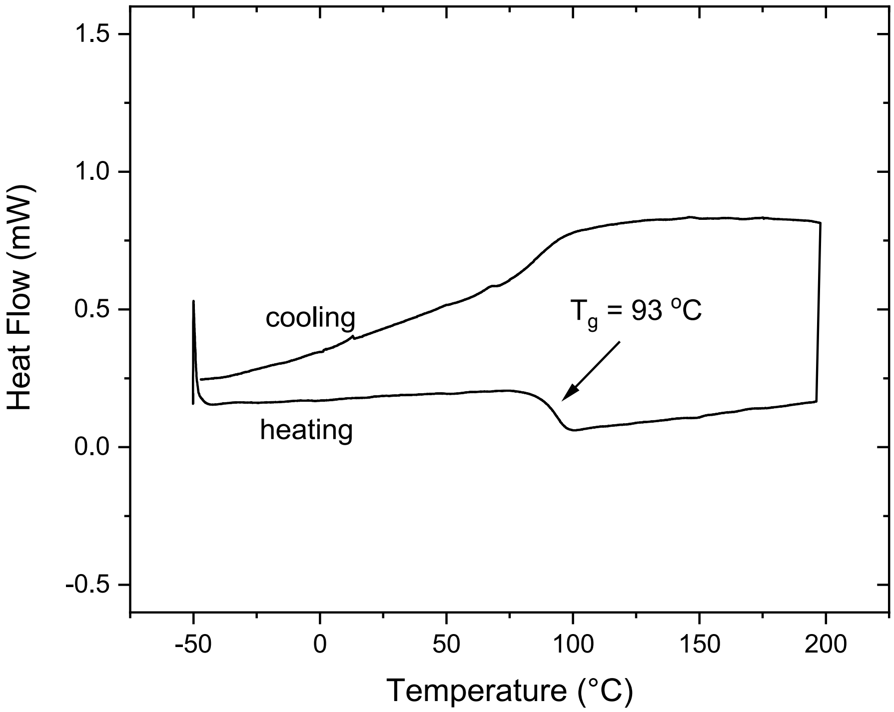

Figure S18. DSC thermogram of poly-**7** at ramp rate of 10 °C/min. The glass transition temperature was determined on the heat run.

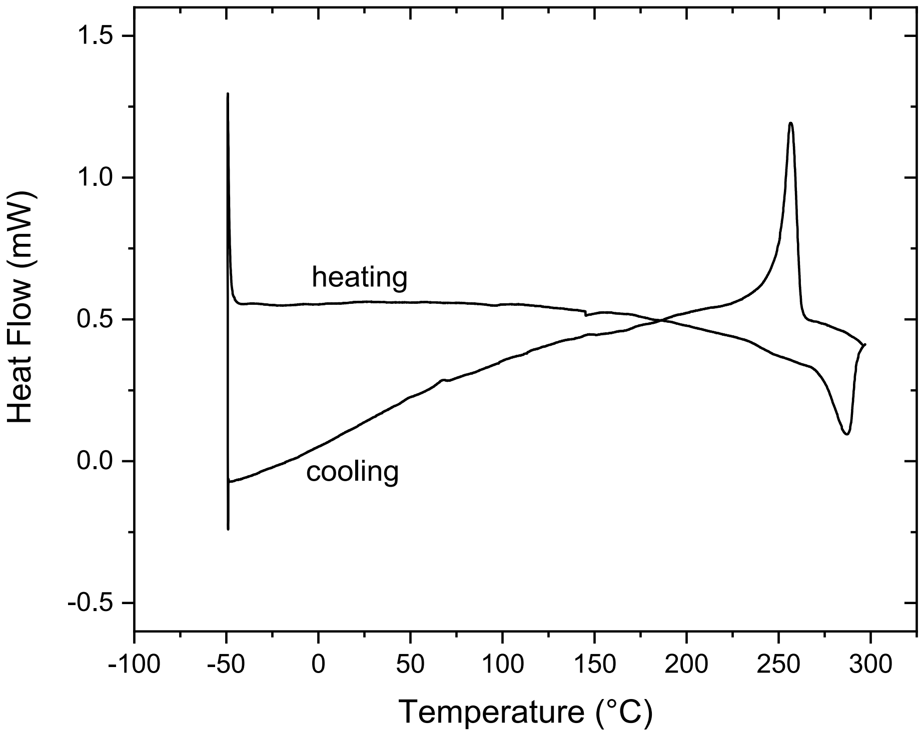

Figure S19. DSC thermogram of oligo-**2** at ramp rate of 10 °C/min. A melting peak is found at 289 °C on the heating run.

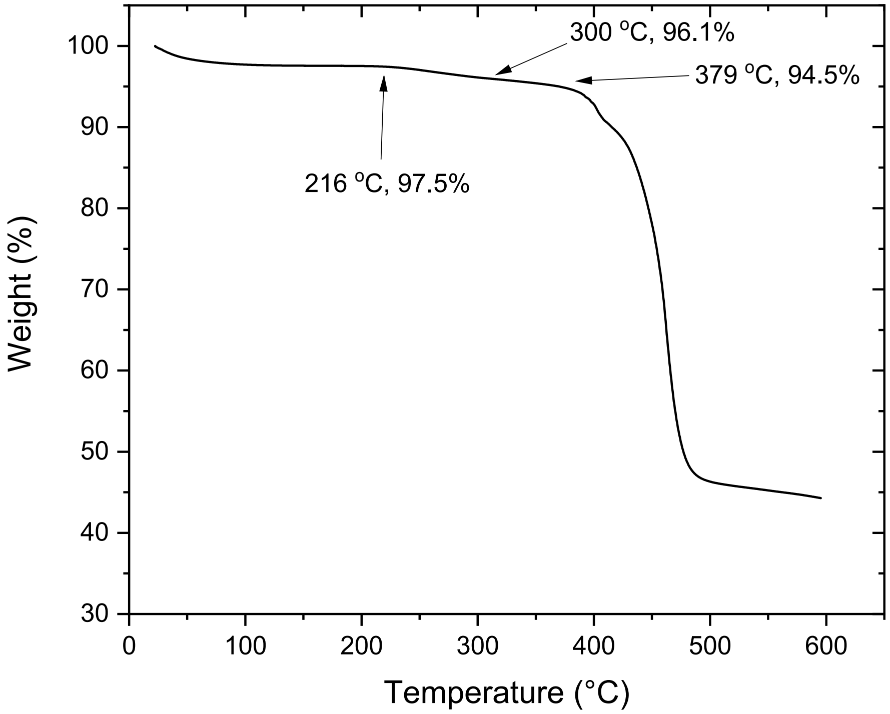

Figure S20. TGA thermogram of oligo-**2** at ramp rate of 10 °C/min. A small weight loss onset at 216 °C which is related to a decomposition process.

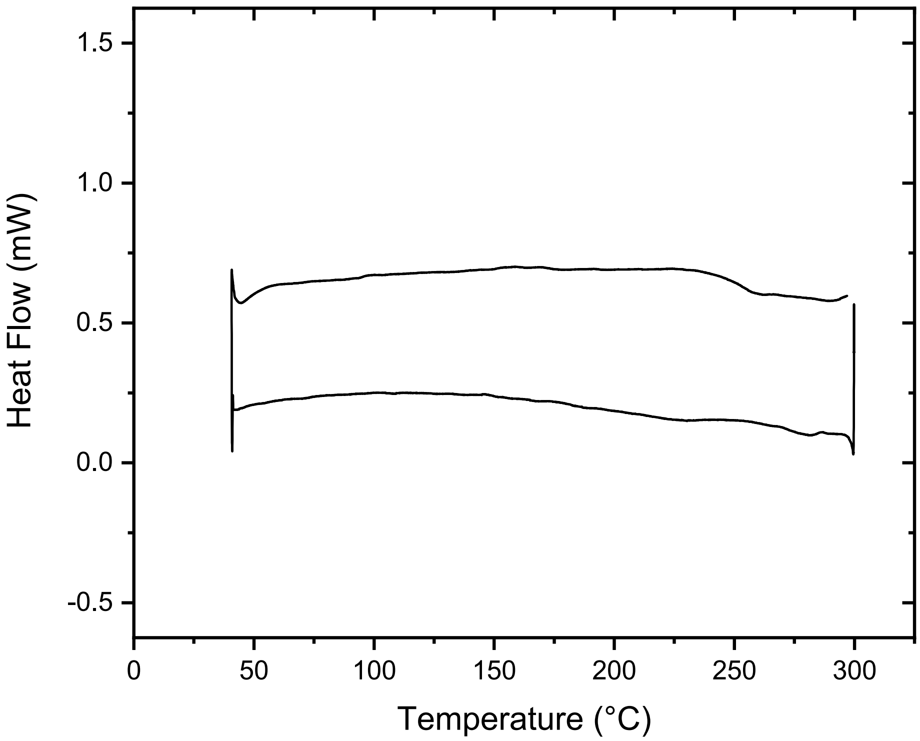

Figure S21. DSC thermogram of LiPSTFSI at ramp rate of 10 °C/min. The T_g was determined to be 256 °C on the heating run.

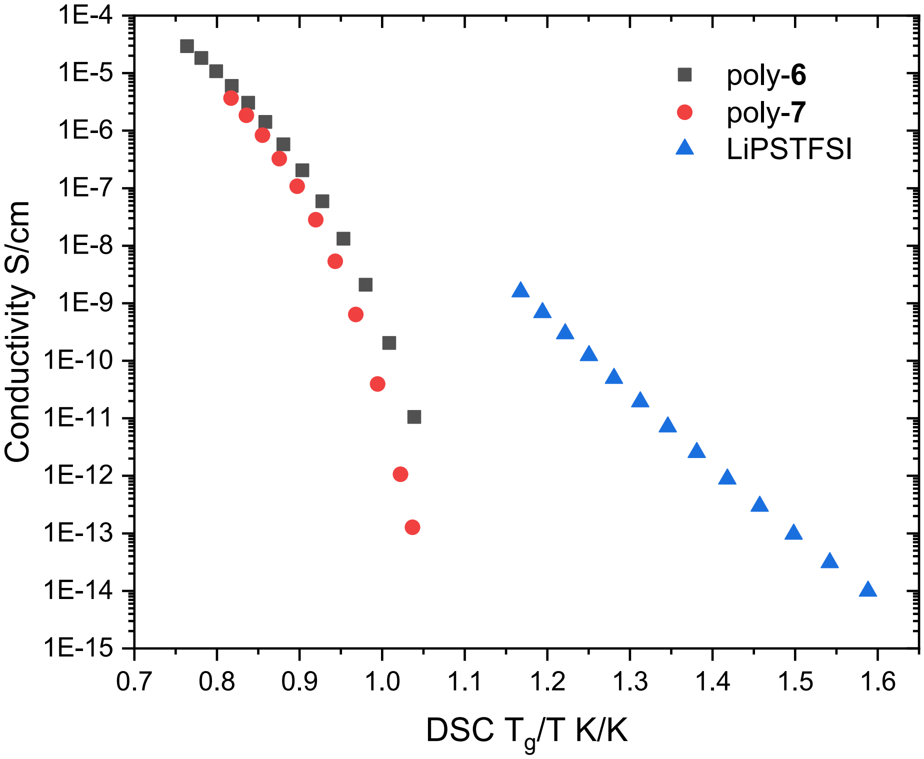

Figure S22. The conductivity curves of poly-**6**, poly-**7,** and LiPSTFSI versus temperature normalized by DSC T_g

Upon normalizing temperature-dependent conductivity against the DSC T_g of poly-**6**, poly-**7**, and LiPSTFSI respectively, the LiPSTFSI curve does not collapse with other two curves which indicates that there is a different transport mechanism. The LiPSTFSI here is in its glassy state at the measurement condition (below 180 °C), and therefore the ion transport mechanism is likely ion hopping rather than a structural relaxation-related mechanism. On this glass transition temperature normalized basis, extrapolation of the data suggests that LiPSTFSI has a higher conductivity relative to poly-**6** and poly-**7** at low T_g normalized temperatures, when all materials are in the glassy state. The exact reason for the faster ion hopping in the glassy LiPSTFSI compared with glassy poly-**6** and poly-**7** is unclear, especially since the chemical composition of the anion is similar, and thus the coordination environment of the Li^+ is expected to be similar. It may be that there is a difference in free volume between the materials.

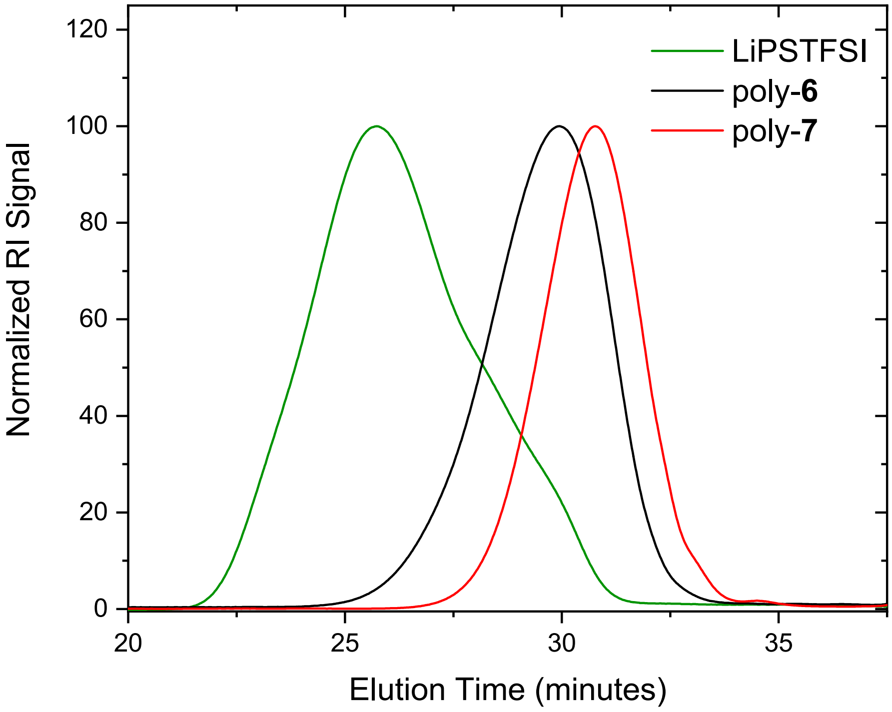

Figure S23. GPC elution profiles of poly-**6**, poly-**7**, and LiPSTFSI. The LiPSTFSI has M_n = 55,700 Da and dispersity = 2.31 against poly(ethylene oxide) standards.

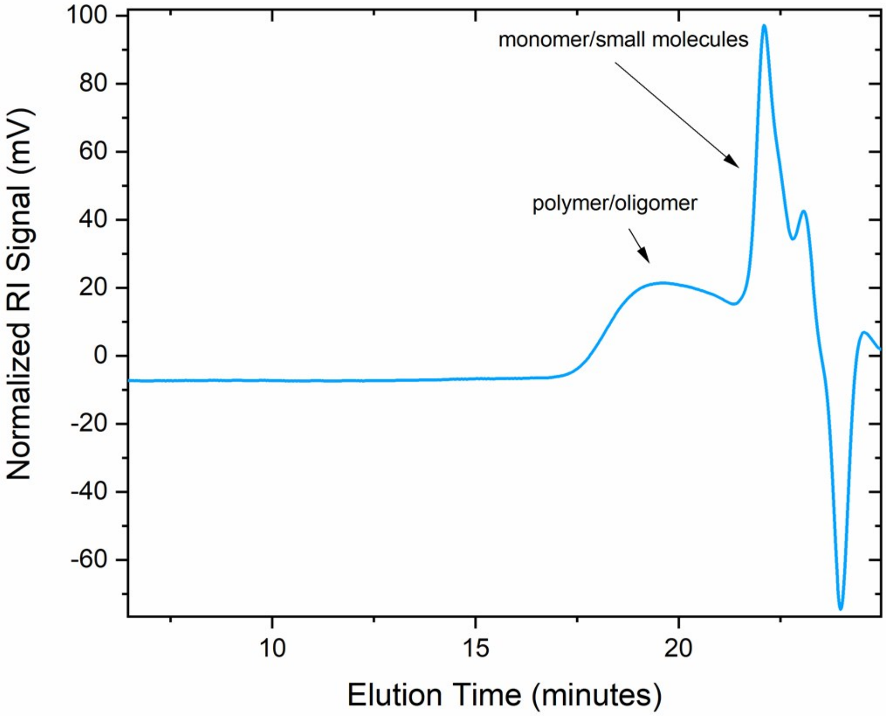

Figure S24. GPC elution profile of oligo-**2**.

The apparent molecular mass calculated from poly(ethylene glycol) calibration standards is Mw = 2300 Da. A secondary, non-resolved peak elutes immediately after the oligo-2, due to remaining small molecules or monomer retained after purification. The negative peak at ≈ 24.5 min is an injection peak due to dissolved gases in the mobile phase. The characteristic peak broadening in the ^{1}H NMR suggests that the oligomers possess at least several repeating units.

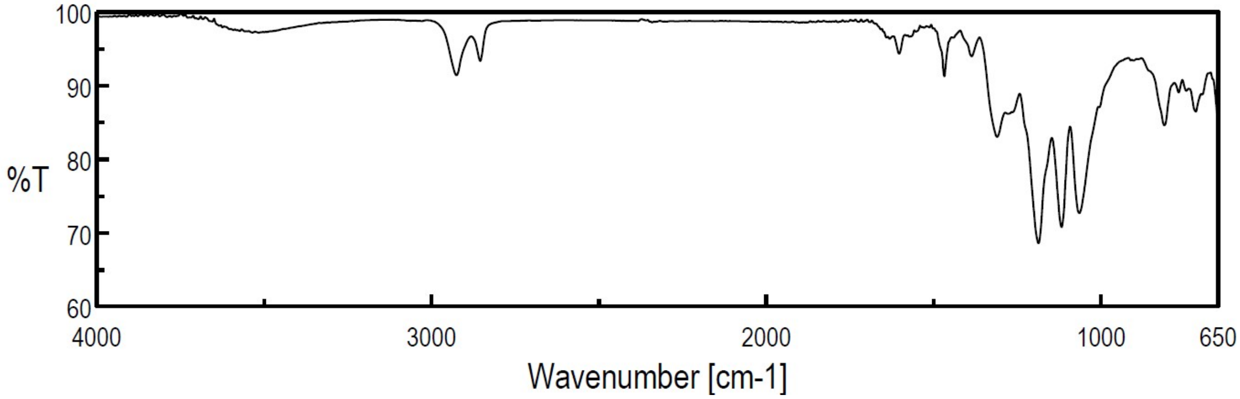

Figure S25. ATR-FTIR spectrum of poly-**6** in terms of percent transmission (% T).

ATR-FTIR (ZnSe, cm^{-1}): 2926, 2856 (C-H stretching), 1603 (C=C stretching), 1468 (C-H bending), 1385 (S=O stretching), 1187 (C-F stretching), 1118 (C-SO2-N bonding mode), 1064 (C-O stretching), 811 (C-H bending), 717 (C=C bending).

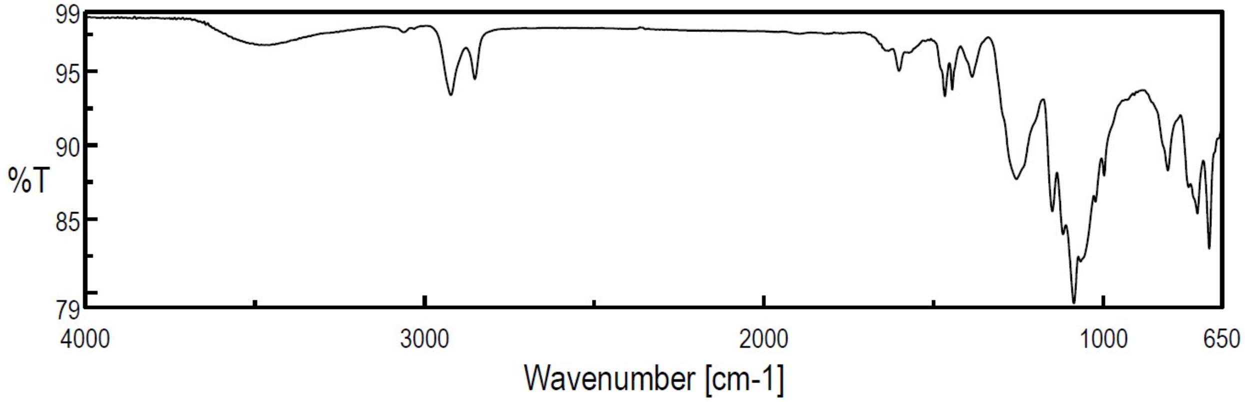

Figure S26. ATR-FTIR spectrum of poly-**7** in terms of percent transmission (% T).

ATR-FTIR (ZnSe, cm^{-1}): 2922, 2852 (C-H stretching), 1602 (C=C stretching), 1467 (C-H bending), 1386 (S=O stretching), 1119 (C-SO2-N bonding mode), 1086 (S-N-S stretching), 1067 (C-O stretching), 809 (C-H bending), 723 (C=C bending).

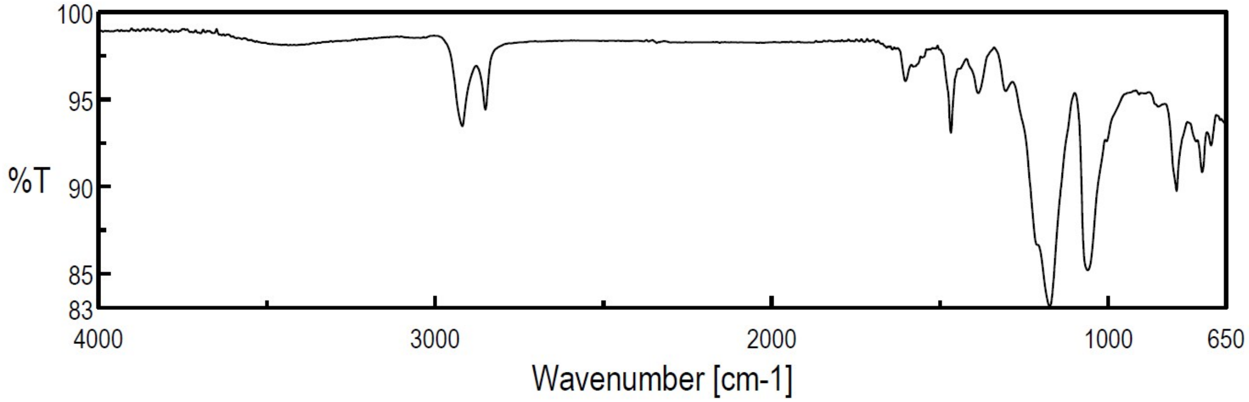

Figure S27. ATR-FTIR spectrum of oligo-**2** in terms of percent transmission (% T).

ATR-FTIR (ZnSe, cm^{-1}): 2920, 2851 (C-H stretching), 1601 (C=C stretching), 1467 (C-H bending), 1385 (S=O stretching), 1175 (S=O stretching), 1061 (C-O stretching), 800 (C-H bending), 722 (C=C bending).